

**Dynamic simulation of capillary breakup of nematic fibers:  
molecular orientation and interfacial rupture**

Chunfeng Zhou<sup>1</sup>, Pengtao Yue<sup>1,2</sup>, James J. Feng<sup>1,2</sup> \*

<sup>1</sup>Department of Chemical and Biological Engineering  
University of British Columbia, Vancouver, BC V6T 1Z3, Canada

<sup>2</sup>Department of Mathematics  
University of British Columbia, Vancouver, BC V6T 1Z2, Canada

**Abstract** - We simulate the breakup of cylindrical fibers of a nematic liquid crystal surrounded by a quiescent Newtonian fluid. The nematic is described by the Leslie-Ericksen theory, and the interfacial motion is captured by a phase-field method from the initial linear instability to final breakup. The focus is on the coupling between liquid crystal molecular orientation and the evolution of the interface. In particular, we examine how molecular anchoring on the interface and orientational distortion in the bulk affect the growth of capillary waves. Results show that the nematic order tends to hinder capillary wave development, in qualitative agreement with prior linear instability analysis. For typical materials, however, the effect becomes prominent only for nano-scale fibers. In addition, anisotropic viscosity plays a significant role in the growth rate of the capillary wave. In the nonlinear stage of the instability, neighboring waveforms grow at different speeds and lead to daughter drops of nonuniform sizes, which typically display the bipolar configuration with two boojum defects. Despite quantitative differences, the breakup of nematic fibers proceeds in mostly the same way as Newtonian ones. The numerical simulations are in general agreement with previous experimental observations.

**Keywords:** Rayleigh instability, drop pinchoff, satellite drops, self-reinforced composites, liquid-crystalline polymers, nanofibers

---

\*Corresponding author. E-mail jfeng@CHML.UBC.CA

## I. INTRODUCTION

Immiscible blends of nematic liquid crystals (LCs) and isotropic liquids occur in several contexts. In optical applications such as polymer-dispersed liquid crystals,<sup>1</sup> the desirable phase morphology is liquid crystal droplets suspended in a polymer matrix. In liquid-crystalline polymer (LCP) composites, on the other hand, it is essential to have the minor LCP phase stretched into thin fibers with strong molecular alignment in the axial direction.<sup>2,3</sup> If the composite is rapidly frozen to retain the fibrous morphology in the solid state, the LCP fibers act as ultra-strong in-situ reinforcement.<sup>4</sup> In addition, LCP *nanofibers*,<sup>5</sup> with diameters on the order of tens of nanometers, form an essential building block in many areas of nanotechnology. Although these are typically electrospun in a gaseous medium, the fiber surface morphology is a central concern as well.<sup>6</sup> More recently, LC filament breakup has been used in microfluidic devices for making monodisperse nematic droplets.<sup>7</sup> The nematic order is a significant determinant of the speed of drop pinchoff and the drop size. Therefore, it is important to understand the capillary stability of the LC fiber and its breakup process.

From a fundamental viewpoint, the breakup of a nematic LC fiber is an interesting process. As the physical dimension of the fiber narrows down to the micro- or nano-meter scale, interfacial effects become increasingly dominant.<sup>8</sup> Aside from the conventional isotropic interfacial tension, the anchoring of LC molecules on the interface contributes in effect an anisotropic part to the interface tension, which may play a significant role in the phase morphology and fluid dynamics of nematic-isotropic two-phase systems.<sup>9,10</sup> This has been illustrated by recent work on bubble and drop behavior in a nematic matrix.<sup>11–13</sup> Typically the coupling between surface anchoring and fluid flow is mediated by bulk elasticity of the LC. For example, enforcing the anchoring condition leads to bulk distortion that modifies the anisotropic rheology of the LC bulk. Evidently, surface anchoring and bulk elasticity are the two major factors governing the energetics of LC-isotropic interfaces. When considering the dissipative dynamics of interfacial deformation and flow, a third factor—anisotropic viscosity—must be considered as well.

Previous experimental work on nematic fiber breakup seems to consist of two qualitative observations of the evolving interface and the birefringent pattern inside the fiber. For a lyotropic liquid-crystalline polymer fiber about 50  $\mu\text{m}$  in initial diameter, Tsakalos

*et al.*<sup>14</sup> reported Rayleigh instability that proceeds much as for Newtonian fluids. Birefringent patterns do reflect effects of the flow field, however, with the uniaxial elongation at the neck producing strong orientational order. Eventually, fiber breakup gives rise to bipolar droplets with a range of sizes. Machiels *et al.*<sup>15</sup> observed similar breakup of thermotropic liquid-crystalline polymer fibers. Neither study was able to shed much light on the coupling between capillary breakup and molecular orientation, and polydomains may have complicated the microstructural order.

Theoretical studies are limited to linear instability analysis based on simplified models. Rey<sup>16</sup> did the first linear analysis on an infinite nematic fiber. The nematic director field  $\mathbf{n}(\mathbf{r})$  is uniform and fixed along the axis of the fiber, unperturbed by the capillary waves. But undulation of the interface forces  $\mathbf{n}$  to deviate from the planar easy direction and is penalized by a Rapini-Papoular anchoring energy.<sup>17</sup> Thus, surface anchoring is accounted for in the weak anchoring limit, since it does not modify the bulk orientation. But in the bulk, Ericksen’s transversely isotropic fluid (TIF) model is used that does not allow distortional elasticity. Results show that the anchoring tends to stabilize the fiber against capillary waves; the threshold for unstable wavelengths is raised and the growth rate of the fastest growing mode is damped when compared with Newtonian fibers of the same viscosity. Similar conclusions were reached by Wang<sup>18</sup> using the Doi theory. Bulk elasticity is omitted, and anchoring is accounted for by an anisotropic surface energy. More recently, Cheong and Rey<sup>19–21</sup> have extended linear analysis to “onion” and radial director fields and non-axisymmetric instability modes.

In spite of the progress made, our theoretical understanding of capillary breakup of nematic fibers suffers from several limitations. First, only linear instability modes have been analyzed, and we have no knowledge of nonlinear growth of capillary waves and the eventual breakup. Second, theoretical analysis has necessitated the use of drastically simplified models. These may capture one or two of the key factors: surface anchoring, bulk elasticity or anisotropic viscosity, but not all three. Finally, the flow field and director field are almost always decoupled to simplify analysis. The motivation for our work is to carry out a fully coupled fluid-dynamic simulation of nematic fiber breakup using the Leslie-Ericksen theory of nemato-hydrodynamics.

The complex rheology of LCs and the need to capture an evolving interface make this a challenging computation. We overcome these difficulties using a finite-element algorithm based on a diffuse-interface model.<sup>22</sup> The methodology was developed for simulating interfacial flows of complex fluids in general. In the current application, we will analyze the effects of surface anchoring, bulk elasticity and anisotropic viscosity separately, with an emphasis on the coupling between nano-scale molecular order and micro-scale fiber morphology.

## II. THEORY AND NUMERICAL METHOD

We treat the nematic-isotropic interface as a thin diffuse layer across which physical properties change rapidly but continuously. The diffuse-interface theory uses a variational formulation based on the free energy of the two-phase system. This is most convenient for the current application where bulk distortion of LCs can be represented by the Frank energy,<sup>23</sup> and surface anchoring by the Rapini-Papoular anchoring energy.<sup>17</sup> Finally, anisotropic viscosity is incorporated by Leslie’s viscous stress tensor. Thus, our algorithm integrates the Leslie-Ericksen theory naturally into an interface-capturing flow solver, bridging the gap between molecular orientation and macroscopic hydrodynamics. Another advantage of the diffuse-interface model, essential to the current simulation, is that it handles topological changes such as interfacial rupture and coalescence rationally via a short-range force resembling the van der Waals force. There is no need for manual intervention as in sharp-interface models to effect such events. The numerical package has been extensively validated,<sup>22</sup> and applied to simulate drop deformation, breakup and coalescence in polymeric and nematic liquids.<sup>9,11,12,24–28</sup> Thus, we will briefly summarize the main ideas in the following, and refer the reader to prior publications for details of the theoretical model and computational algorithm.

We employ a scalar phase field  $\phi(\mathbf{r})$  to represent the composition of a Newtonian-nematic two-component system. The Newtonian bulk is represented by  $\phi = -1$  and the nematic by  $\phi = 1$ , and the interfaces are simply the level set of  $\phi = 0$ . The governing equations are the continuity and momentum equations, supplemented by the Cahn-Hilliard equation for

the transport of the phase field  $\phi$  and the Leslie-Ericksen equations of nematohydrodynamics:<sup>12,24</sup>

$$\nabla \cdot \mathbf{v} = 0, \quad (1)$$

$$\rho \left( \frac{\partial \mathbf{v}}{\partial t} + \mathbf{v} \cdot \nabla \mathbf{v} \right) = -\nabla p + \nabla \cdot \boldsymbol{\sigma}, \quad (2)$$

$$\frac{\partial \phi}{\partial t} + \mathbf{v} \cdot \nabla \phi = \gamma \lambda \nabla^2 \left[ -\nabla^2 \phi + \frac{\phi(\phi^2 - 1)}{\epsilon^2} \right], \quad (3)$$

$$\mathbf{h} = \gamma_1 \mathbf{N} + \gamma_2 \mathbf{D} \cdot \mathbf{n}, \quad (4)$$

where  $\lambda$ ,  $\epsilon$  and  $\gamma$  are the interfacial energy density, capillary thickness and mobility of the diffuse interface, respectively. The density  $\rho = \frac{1+\phi}{2}\rho_1 + \frac{1-\phi}{2}\rho_2$  is an average between the two components. The stress tensor  $\boldsymbol{\sigma}$  in the momentum equation is:

$$\boldsymbol{\sigma} = -\lambda \nabla \phi \nabla \phi - K \frac{1+\phi}{2} \nabla \mathbf{n} \cdot (\nabla \mathbf{n})^T - \mathbf{G} + \frac{1+\phi}{2} \boldsymbol{\sigma}' + \frac{1-\phi}{2} \mu [\nabla \mathbf{v} + (\nabla \mathbf{v})^T], \quad (5)$$

where  $K$  is the Frank elastic constant of the bulk nematic under the one-constant approximation, and  $\mu$  is the Newtonian viscosity.  $\mathbf{G}$  is the anchoring stress of the nematic director on the interface,  $\mathbf{G} = A(\mathbf{n} \cdot \nabla \phi) \mathbf{n} \nabla \phi$  for planar anchoring,  $A$  being the surface anchoring energy density. Homeotropic anchoring can be readily modeled but is not as relevant here since stretched LC fibers tend to have  $\mathbf{n}$  aligned axially.<sup>14,16</sup>  $\boldsymbol{\sigma}'$  is the Leslie viscous stress<sup>29</sup> in the nematic phase

$$\boldsymbol{\sigma}' = \alpha_1 \mathbf{D} : \mathbf{n} \mathbf{n} \mathbf{n} \mathbf{n} + \alpha_2 \mathbf{n} \mathbf{N} + \alpha_3 \mathbf{N} \mathbf{n} + \alpha_4 \mathbf{D} + \alpha_5 \mathbf{n} \mathbf{n} \cdot \mathbf{D} + \alpha_6 \mathbf{D} \cdot \mathbf{n} \mathbf{n}, \quad (6)$$

where  $\alpha_{1-6}$  are the Leslie viscous coefficients obeying an Onsager relation  $\alpha_2 + \alpha_3 = \alpha_6 - \alpha_5$  so five of them are independent.<sup>23</sup>  $\mathbf{D} = \frac{1}{2}[\nabla \mathbf{v} + (\nabla \mathbf{v})^T]$  is the strain rate tensor,  $\boldsymbol{\Omega} = \frac{1}{2}[(\nabla \mathbf{v})^T - \nabla \mathbf{v}]$  is the vorticity tensor, and  $\mathbf{N} = \frac{d\mathbf{n}}{dt} - \boldsymbol{\Omega} \cdot \mathbf{n}$  is the rotation of  $\mathbf{n}$  with respect to the background flow field. The director field  $\mathbf{n}$  evolves in the flow field according to a balance between elastic and viscous torques as given in Eq. (4). The molecular field  $\mathbf{h}$ , denoting elastic torque in the nematic, derives from the free energies of the system:<sup>23</sup>

$$\mathbf{h} = K \left[ \nabla \cdot \left( \frac{1+\phi}{2} \nabla \mathbf{n} \right) - \frac{1+\phi}{2} \frac{(\mathbf{n}^2 - 1) \mathbf{n}}{\delta^2} \right] - \mathbf{g}, \quad (7)$$

with  $\mathbf{g} = A(\mathbf{n} \cdot \nabla \phi) \nabla \phi$  for planar anchoring. The term involving  $\delta$  arises from an energy penalty added to the Frank energy to allow defects to be represented by reduced  $|\mathbf{n}|$  values

within a small area of size  $\delta$ .<sup>30</sup> Thus,  $|\mathbf{n}|$  acts like a local order parameter, and the model closely resembles Ericksen’s generalization of the Leslie-Ericksen theory by a variable order parameter.<sup>31</sup> We have used  $\delta = 4\epsilon$  since the defect core size is comparable to the interfacial thickness. Note that in the limit of  $\epsilon \rightarrow 0$ , the diffuse interface model reduces to the classic sharp-interface hydrodynamics.<sup>24</sup> In particular, the interfacial tension  $\sigma$  and Rapini-Papoular anchoring constant  $W$  can be recovered from the diffuse-interface parameters for small  $\epsilon$ :  $\sigma = 2\sqrt{2}\lambda/3\epsilon$  and  $W = 2\sqrt{2}A/3\epsilon$ . To faithfully approximate the sharp-interface limit,  $\epsilon$  needs to be  $O(10^{-2}a)$ ,  $a$  being the macroscopic length scale of typical problems.

Although non-axisymmetric instability modes have been considered before,<sup>20</sup> experiments have shown only axisymmetric capillary waves and drop pinchoff.<sup>7,14,15</sup> Thus, we will assume axisymmetry throughout this study. The governing equations are discretized on a unstructured grid of triangular elements using the Petrov-Galerkin formulation.<sup>22</sup> A critical ingredient of the algorithm is an adaptive meshing scheme that accurately resolves the evolving interface and any orientational defects. Typical grid sizes are  $h_1 = 0.006a$  at the interface and near defects,  $h_2 = 0.2a$  inside the fiber and  $h_3 = 0.5a$  in the matrix, with smooth transitions between different regions. Time integration is by an implicit second-order scheme with the time step automatically adjusted according to the motion of the interface. Numerical experiments have shown that the grid sizes and the time step used in the simulations are sufficient for numerical convergence.

### III. RESULTS AND DISCUSSIONS

The geometry of the axisymmetric computational domain is shown in Fig. 1, with the nematic LC fiber surrounded by a quiescent Newtonian fluid. We apply periodic boundary conditions along the  $z$  direction, and no slip boundary conditions on the outer boundary ( $r = R$ ). On the axis of symmetry  $r = 0$ ,  $\mathbf{n}$  is in the  $z$  direction and the radial velocity vanishes. Note that the velocity, stress and anchoring conditions on the nematic-isotropic interface have been embedded into the diffuse-interface formulation and do not constitute boundary conditions. Initially both phases are at rest, the interface is a perfect cylinder and the molecular orientation is uniform and axial inside the fiber. Surface disturbances arise spontaneously from numerical noise.

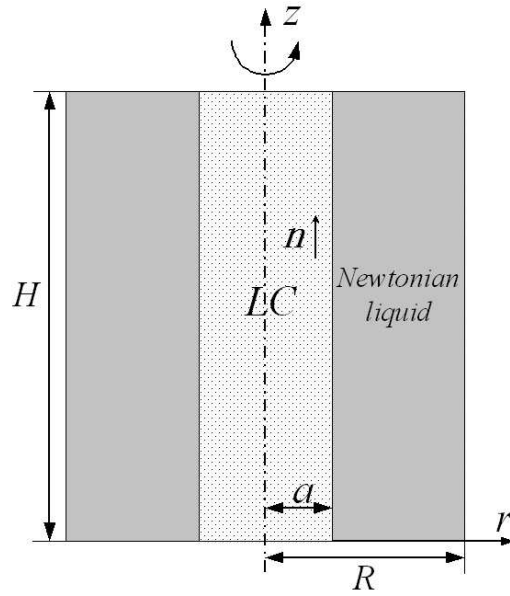


Figure 1: Schematic of the computational domain, which is half of the meridian plane of the axisymmetric geometry.

Most results presented are for a domain length  $H = 25a$  and width  $R = 3.33a$ . Since the dominant capillary wavelength is not known *a priori*, and in any event varies with the physical parameters, imposing periodicity over a finite  $H$  necessarily introduces errors to the result. Comparison with simulations in longer domains, with  $H$  up to  $60a$ , shows that  $H$  affects the results quantitatively but does not modify the qualitative trend. Thus,  $H = 25a$  represents a tradeoff between computational cost and accuracy. For Newtonian fluids, the confinement effect of the outer boundary on capillary instability of a filament has been studied by Mikami and Mason.<sup>32</sup> For  $R = 3.33a$ , the growth rate of the dominant mode should decrease by approximately 10%. For our nematic fiber, comparing the result with that in a wider domain with  $R = 10a$  shows that the confinement reduces the growth rate by 4.6%. Therefore, the finite size of the computational domain, while exerting a quantitative influence, does not hinder the main purpose of the simulations.

The complete set of dimensionless groups governing our system is:

$$\alpha = \frac{\rho_1}{\rho_2} \quad (\text{nematic-to-matrix density ratio}), \quad (8)$$

$$\beta = \frac{\alpha_4/2}{\mu} \quad (\text{nematic-to-matrix viscosity ratio}), \quad (9)$$

$$A_K = \frac{K}{\sigma a} \quad (\text{bulk elasticity-to-interfacial tension ratio}), \quad (10)$$

$$A_W = \frac{W}{\sigma} \quad (\text{anchoring-to-interfacial tension ratio}), \quad (11)$$

$$Ca = \frac{\eta U}{\sigma} \quad (\text{capillary number}), \quad (12)$$

$$Re = \frac{\rho_1 U a}{\eta} \quad (\text{Reynolds number}), \quad (13)$$

along with the various length ratios of the geometry and ratios between the Leslie viscous coefficients.  $Re$  and  $Ca$  are defined using the visco-capillary velocity  $U = \sigma/\eta$ . Therefore the capillary number is 1, and the Reynolds number is kept at 150 throughout this study. Note that the typical velocity during the fiber breakup is roughly 1% of  $U$ , and the actual  $Ca$  and  $Re$  are much smaller. The viscosity  $\eta = (\alpha_3 + \alpha_4 + \alpha_5)/2$  is the average between the largest and smallest Miesowicz viscosities.<sup>23</sup> The ratio  $\alpha_3/\alpha_2$  determines whether the nematic “tumbles” or “flow-aligns” in simple shear flows. But the distinction is unimportant here as fiber breakup engenders predominantly elongational flows. Thus we adopt the Leslie viscosities of a common nematic MBBA at 25°C as the basis for the computations:<sup>23</sup>  $\alpha_1 = 6.5$  centipoise (cp),  $\alpha_2 = -77.5$  cp,  $\alpha_3 = -1.2$  cp,  $\alpha_4 = 83.2$  cp,  $\alpha_5 = 46.3$  cp,  $\alpha_6 = -32.4$  cp. Furthermore, we match the density and isotropic viscosity of the nematic with the surrounding fluid:  $\alpha = 1$ ,  $\beta = 1$ . In the following subsections, we study the effects of the bulk elasticity, interface anchoring and anisotropic viscosity in turn, by varying  $A_K$ ,  $A_W$  and the viscosity ratios, respectively.

### A. Bulk elasticity

With the anchoring energy fixed at  $A_W = 1$ , Fig. 2 compares the development of capillary waves at different strengths of bulk elasticity. Note that the baseline case (Fig. 2a) is not for a Newtonian fluid; the fiber still retains the same anisotropic viscosity and surface anchoring. In our periodic domain of length  $25a$ , the dominant mode has three wave forms, with a wavelength of  $8.33a$ . In comparison, an infinitely long Newtonian fiber of the same viscosity would have a fastest growing wavelength of  $9.66a$  according to Mikami

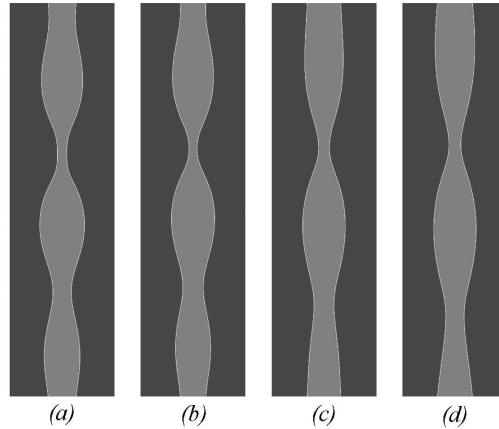


Figure 2: Effect of bulk elasticity on capillary waves on a nematic fiber. The domain is  $25a$  in length and  $6.66a$  in width. The viscosity coefficients are those of MBBA, and surface anchoring is fixed at  $A_W = 1$ . The bulk elasticity  $K$  increases from left to right: (a)  $A_K = 0$ ,  $t = 491$ ; (b)  $A_K = 0.0167$ ,  $t = 497$ ; (c)  $A_K = 0.833$ ,  $t = 547$ ; (d)  $A_K = 1.67$ ,  $t = 575$ . Time is made dimensionless by  $\eta a/\sigma$ .

and Mason’s model.<sup>32</sup> For a nematic fiber with a weak bulk elasticity,  $A_K = 0.0167$ , the modification to the dominant wavelength is too small to be manifested, and the three wave forms persist (Fig. 2*b*). At  $A_K = 0.833$ , however, the dominant wavelength has lengthened to  $12.5a$  with two wave forms (Fig. 2*c*). Further doubling the bulk elasticity to  $A_K = 1.67$  does not change the wavelength in Fig. 2(*d*).

One observation is that bulk elasticity tends to increase the wavelength of the capillary waves. This is in qualitative agreement with the predictions of linear stability analysis. Cheong and Rey<sup>21</sup> showed that the fastest growing wavelength on an infinitely long inviscid nematic fiber is

$$\lambda_{max} = 2\sqrt{2}\pi a\sqrt{1 + 2A_K}, \quad (14)$$

which reduces to Rayleigh’s classical result for an inviscid fiber at  $K = 0$ . This formula predicts that the bulk elasticity would increase  $\lambda_{max}$  by 1.7%, 63% and 108% for the three cases in Fig. 2(*b–d*), which is consistent with the numerical results considering the constraint of the forced periodicity over  $H = 25a$ . However, further increasing  $A_K$  up to 10 does not produce a single wave form in our domain, as expected from the linear formula above. We will return to this discrepancy shortly. A second observation is that the bulk elasticity tends to dampen the growth of the capillary waves. The four panels in Fig. 2 correspond to roughly the same wave amplitude. The time needed for reaching this amplitude increases

with increasing  $A_K$ . Again, this may be compared with the linear growth rate on an inviscid nematic fiber:<sup>21</sup>

$$\alpha_{max} = \frac{\sqrt{\frac{\sigma}{8\rho a^3}}}{\sqrt{1 + 2A_K}}. \quad (15)$$

For our three cases (Fig. 2*b–d*), this predicts a reduction in  $\alpha_{max}$  of 2%, 39% and 52%, respectively. The actual damping of the growth rate in the simulations is smaller in magnitude: 1.2%, 10% and 15% for the three cases.

It is perhaps unreasonable to expect a closer correspondence between our numerical results and Eqs. (14) and (15). Besides the aforementioned constraints of  $H = 25a$ ,  $R = 3.33a$  and the nonlinear nature of our results, the physical models differ in that Cheong and Rey<sup>21</sup> assumed inviscid fibers and rigid anchoring on the interface. Rigid anchoring tends to amplify the effects of bulk elasticity since it couples the interfacial deformation to bulk distortion more directly, without the “buffering” effect of the anchoring energy. Therefore, it is not surprising that in our simulations using a finite  $W = \sigma$ , the dominant wavelength does not increase as much as predicted by Eq. (14), and the growth rate does not decrease as much as predicted by Eq. (15).

A *nonlinear* feature of Fig. 2 is that the waves are not precisely periodic along the axial direction. The thinning of the fiber proceeds more rapidly at the upper “neck” than the lower. This can be easily understood from the capillary pressure in the fiber. Let us assume that two neighboring wave forms are initially identical. The high capillary pressure at the neck drives the fluid toward the crest of the wave. If some small disturbance should slightly delay the thinning of one neck relative to the next, the thinner neck experiences a greater capillary pressure that more effectively pumps fluid away, thereby further widening the difference between the two necks. Thus, the uneven growth among the waveforms is a natural outcome of capillary instability. This behavior has been observed in Newtonian<sup>33</sup> and nematic fiber breakup experiments,<sup>14,15</sup> and is related to “volume scavenging” between coupled spherical-cap droplets.<sup>34</sup> As a result, polydisperse drops are produced. To produce monodisperse droplets, one can resort to strongly elongational flows, as have been used in microfluidic devices.<sup>7,27</sup>

Figure 3 depicts the late stage of fiber breakup for a nematic fiber with  $A_K = 0.0167$  and  $A_W = 1$ . Since  $A_W/A_K = Wa/K \gg 1$ , one expects the anchoring effect to dominate

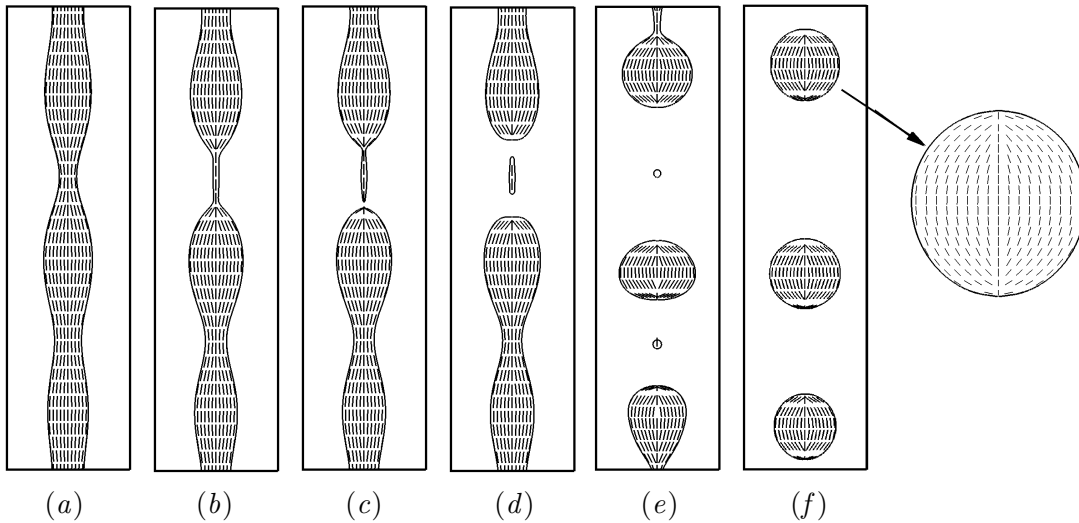


Figure 3: Evolution of the interface and the director field during breakup.  $A_W = 1.0$ ,  $A_K = 0.0167$ . The snapshots are at different times: (a)  $t = 476$ , (b) 502, (c) 507, (d) 512, (e) 566, (f) 658. Note that  $\mathbf{n}$  is shown only on a small number of interpolation points; the finite-element mesh is much denser.

the bulk elasticity in determining the director field.<sup>11</sup> Indeed, throughout the breakup process,  $\mathbf{n}$  follows the undulation of the interface except near the centerline, where the elongational flow aligns  $\mathbf{n}$  axially. The same elongational flow stretches the neck into a thread (Fig. 3b), which then pinches off at both ends to form a satellite drop between the two daughter drops (Fig. 3c-d). The pinchoff produces pointed tips where the director field converges. The high curvature there induces a large capillary force that pulls the tips back sharply, giving rise to flat ends (Fig. 3d) or even flattened drops (Fig. 3e). In the meantime, the converging director field develops “boojums” defects at the ends. Finally, the thread breaks up into three primary droplets and three satellite droplets. The drops display a bipolar configuration (Fig. 3f) with two boojums at the poles. The shape is nearly spherical in this case, but becomes more prolate with increasing  $A_W$  and  $A_K$ , similar to previous observations.<sup>9</sup> As anticipated earlier, the primary drops are not monodisperse; the bottom drop is some 5.7% smaller than the other two. Note also that the satellite drops shrink in time and eventually disappear owing to the Cahn-Hilliard diffusion. The implications of this diffuse-interface phenomenon has been examined at length.<sup>35</sup>

The nematic fiber breakup process, as simulated and discussed above, may be compared with experimental observations.<sup>14,15</sup> First, the simulation and experiments agree in that

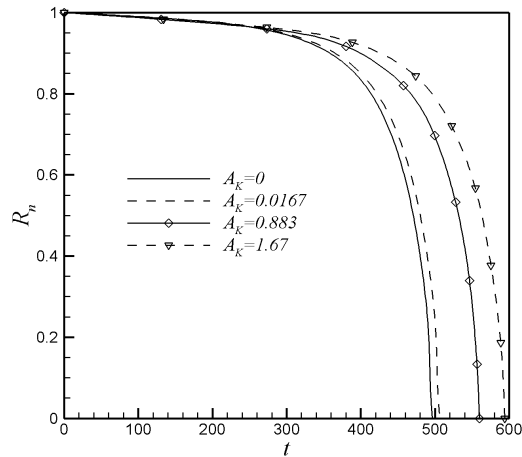


Figure 4: Thinning of the minimum neck radius at different levels of bulk elasticity.

the breakup of a nematic fiber *does not differ markedly* from that of a Newtonian fiber. The uneven wave growth, the pinchoff at the neck and even the formation of satellite drops are qualitatively the same as in Newtonian fluids.<sup>36</sup> There is nothing as spectacular as, say, the bead-on-string morphology for highly viscoelastic polymeric threads.<sup>37</sup> Quantitatively, the nematic order makes the breakup proceed more slowly, and we will amplify this point shortly in connection to the thinning of the neck. Second, the general features of the experiments are captured by the simulations, including the highly aligned  $\mathbf{n}$  field at the necks, the formation of satellite drops, the bipolar configuration and the polydispersity of the primary drops.<sup>14</sup> Finally, there are a few observations that the computation fails to reproduce. For instance, a “banded structure”, visible through crossed polarizers, sometimes emerges prior to capillary instability.<sup>14</sup> This is probably due to the relaxation of the molecular order that has been elevated during the formation of the fibers by stretching. Our Leslie-Ericksen theory does not account for such molecular relaxation. Furthermore, thermotropic LCP fibers often break up into spherical drops containing polydomains whose disordered orientation renders the drop essentially isotropic on the whole.<sup>15,38</sup> The origin of defects and polydomains is a long-standing problem in LCP dynamics, and requires more sophisticated models than that used here.

To examine more quantitatively the effect of bulk elasticity on the breakup process, we plot in Fig. 4 the minimum neck radius  $R_n$  for several values of  $A_K$ , which decreases

in time until pinchoff. Interestingly, the initial growth of the capillary waves ( $t < 300$ ) is little influenced by the differing bulk elasticity. At the beginning of the simulations, the nematic director  $\mathbf{n}$  is aligned axially in the bulk and tangentially on the interface, which induces neither bulk elastic energy nor surface anchoring energy. As the capillary wave develops, surface undulation causes both surface and bulk distortion and the energy penalties amount to an elastic force that resists the growth of the capillary wave. This is the explanation for the stabilizing effects of the nematic order. As a reaction to interfacial deformation, however, the effect only becomes significant as the capillary wave reaches a certain amplitude. As measured in Fig. 4, the amplitude is only about  $0.05a$  at  $t = 300$ , and thus the director field has yet to exert a significant effect on the capillary wave development. Later, with growing capillary waves, the interfacial and bulk distortion continue to absorb some of the energy released from interfacial area reduction. As a result, less is available to drive capillary breakup against viscous dissipation and inertia. This explains the longer pinchoff time for larger  $A_K$  values in Fig. 4.

Finally, it is important to note that real liquid crystals typically have a weak  $K \sim 10^{-11}$  N.<sup>23</sup> With a surface tension  $\sigma \sim 10^{-3}$  N/m,<sup>39,40</sup> for example,  $A_K = 0.01$  for a fiber 1  $\mu\text{m}$  in radius. Thus, LC bulk elasticity plays a significant role only for *nanofibers*, such as produced by electrospinning.<sup>5,6</sup> However, certain lyotropic systems possess exceedingly low interfacial tensions,<sup>41</sup> for which bulk elasticity effect may be manifested at larger length scales.

## B. Interface anchoring

We have chosen to discuss bulk elasticity and surface anchoring separately, but obviously the two must cooperate for either to have an effect. It is perhaps appropriate to say that the surface anchoring communicates interfacial deformation to the director field in the bulk. In previous linear instability analyses, Rey<sup>16</sup> isolated the effect of surface anchoring by making the bulk elasticity infinitely strong, and Cheong and Rey<sup>21</sup> isolated the effect of bulk elasticity by making surface anchoring rigid. In this subsection, we fix bulk elasticity at  $A_K = K/\sigma a = 0.833$ , and vary the anchoring strength through  $A_W = W/\sigma$ .

The effect of  $A_W$  is illustrated by Table 1 that compares the wavelength and pinchoff time for  $A_W$  values ranging from 0 to 10. Thus, the surface anchoring tends to raise

$A_W$	0	0.1	0.5	1	2	5	10	Newtonian
Wavelength	8.33a	8.33a	8.33a	12.5a	12.5a	12.5a	12.5a	8.33a
pinchoff time	520	524	536	560	614	638	704	686

Table 1: Wavelength and pinchoff time at various surface anchoring energies, with  $A_K = 0.833$ ,  $Ca = 1$  and  $Re = 150$ . Time is made dimensionless by  $\eta a/\sigma$ . The last column, for an isotropic Newtonian fluid with a viscosity equal to the average viscosity  $\eta$  of the LC’s, will be cited in the next subsection.

the threshold wavelength for unstable modes, and reduce their growth rates. In terms of hindering the growth of capillary instability,  $A_W$  is similar to  $A_K$ . This is no surprise because, as we alluded to above, the surface anchoring and bulk distortion are allied in bringing about the stabilizing effect on capillary waves.

For an infinite nematic fiber with  $A_K = \infty$  but a finite  $A_W$ , Rey’s analysis<sup>16</sup> gives the fastest growth wavelength

$$\lambda = 2\sqrt{2}\pi a \sqrt{1 + A_W + 2\sqrt{\frac{Ca}{Re}} \sqrt{1 + A_W}} \quad (16)$$

and the fastest growth rate

$$\alpha_{max} = \sqrt{\frac{\sigma}{8\rho a^3}} \frac{1}{\sqrt{1 + A_W} + \sqrt{\frac{Ca}{Re}}}. \quad (17)$$

For  $Ca = 1$ ,  $Re = 150$  and  $A_W = 1$ , for example, the above formulae predict a 49% increase of the fastest-growing wavelength due to the interface anchoring, and a 34% decrease of its growth rate. Table 1 gives, for the corresponding conditions, a 50% lengthening of the wavelength and 7.1% decrease in the growth rate (estimated from the inverse of the total pinchoff time). Considering the differences in the physical models, parameters and geometric setup, the qualitative agreement is reasonable. Wang<sup>18</sup> carried out a similar normal mode analysis using the Doi theory for liquid-crystalline polymers in the limit of vanishing bulk elasticity. At a capillary number of unity, with  $A_W$  increasing from 0 to 10, the most dangerous wavelength is roughly doubled, and its grow rate decreases by 40%. These numbers are again consistent with our results in Table 1.

The later stage of the fiber breakup process does not vary qualitatively for the  $A_W$  range simulated. Necking, drop pinchoff and satellite drop formation are similar to those depicted

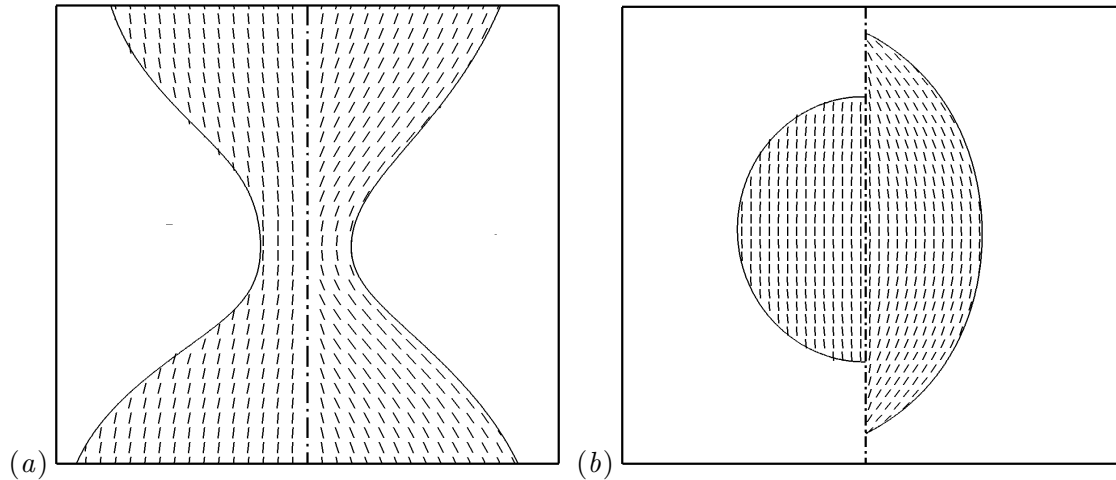


Figure 5: Effect of  $A_W$  on the director field (a) inside the fiber during breakup and (b) inside a daughter drop. The radial dimension in (a) is amplified by a factor of 3 for a clearer view. In each plot, the left image corresponds to weak anchoring at  $A_W = 0.1$ , with time  $t = 113$  in (a) and  $t = 694$  in (b), while the right to  $A_W = 6$  with  $t = 170$  in (a) and  $t = 780$  in (b). All other parameters are the same as in Table 1.

in Fig. 3. In fact, these features are basically the same as in Newtonian fiber breakup, as noted in previous experimental observations.<sup>14,15</sup> But the molecular orientation inside the fiber and later inside the drops does reflect the anchoring strength as shown in Fig. 5. For weak anchoring,  $\mathbf{n}$  readily deviates from the easy direction on the interface so as to avoid comparatively expensive bulk distortions. During the growth of capillary waves (Fig. 5a), therefore, the interfacial undulation only affects the outer layer of the nematic. In the daughter drops that result from the breakup (Fig. 5b),  $\mathbf{n}$  does not nucleate boojum defects on the surface but maintains a relatively uniform orientation. For strong anchoring, the interfacial contour has a much greater impact on the bulk  $\mathbf{n}$  field, both in the fiber and the final bipolar daughter drops.

### C. Anisotropic viscosity

The foregoing discussion on anchoring and bulk elasticity concern *energetic* interactions. In the later stage of breakup, fluid flow introduces considerable dissipation into the system. Thus, anisotropic viscosity, a key rheological feature of nematic LCs, becomes a factor in the development of finite-amplitude capillary waves and final breakup. In fact, that is why in the preceding subsections, we compared the nematic fibers not against an *isotropic*

*Newtonian* baseline, but one with nil bulk or anchoring energy and the same anisotropic viscosity. The latter being kept the same, the effects of  $A_K$  and  $A_W$  were thus isolated. For a truly Newtonian fiber with an isotropic viscosity matching the LC average viscosity  $\eta$ , the pinchoff time is 686 in Table 1. Comparing this with the nematic fibers having  $A_W = 0$  and  $A_W = 10$  in the same table, it is apparent that the viscous anisotropy may have as great an effect on LC fiber breakup as  $A_W$  (and  $A_K$ ). To quantify this systematically, we fix the surface anchoring and bulk elasticity at  $A_\sigma = 1$  and  $A_K = 0.833$  and vary the degree of viscous anisotropy through the Leslie coefficients. Note that this is essentially a nonlinear effect in that it does not affect the initial stages of linear instability.

Given the five independent Leslie coefficients, it is not obvious how to quantify viscous anisotropy. In simple shear flows, a convenient gauge is the Miesowicz viscosities measured with the director  $\mathbf{n}$  uniformly fixed perpendicular or parallel to the flow direction:<sup>12,23</sup>

$$\eta_\perp = \frac{-\alpha_2 + \alpha_4 + \alpha_5}{2}, \quad (18)$$

$$\eta_\parallel = \frac{\alpha_3 + \alpha_4 + \alpha_6}{2}. \quad (19)$$

Borrowing the same idea to the fiber breakup problem, we have kept the average LC viscosity  $\eta = (\eta_\perp + \eta_\parallel)/2$  constant, and varied the viscous anisotropy via the ratio  $\nu = \eta_\perp/\eta_\parallel$ . Using the Onsager relationship  $\alpha_2 + \alpha_3 = \alpha_6 - \alpha_5$ , we rewrite  $\nu$  as

$$\nu = \frac{2\eta - \alpha_2 - \alpha_3}{2\eta + \alpha_2 + \alpha_3} = \frac{4\eta}{2\eta + \alpha_2 + \alpha_3} - 1, \quad (20)$$

which shows that  $\nu$  can be manipulated via either  $\alpha_2$  or  $\alpha_3$ . To keep  $\eta$  constant,  $\alpha_6$  or  $\alpha_5$  have to be adjusted accordingly. In the following, we vary  $\alpha_2$  or  $\alpha_3$  on the basis of the Leslie coefficients of MBBA, which has  $\eta = 64.15$  cp and  $\nu = 4.34$ .

Figure 6 plots thinning of the neck radius for various degrees of viscous anisotropy. First, note that in the parameter ranges explored, the effect of  $\nu$  on the pinchoff time is comparable to that of  $A_K$  (Fig. 4) and  $A_W$  (Table 1). With varying  $\alpha_2$ , Fig. 6(a) shows a monotonic trend, with the fiber breaking up faster for larger  $\nu$  (or smaller  $\alpha_2$ ). Naively, one might rationalize this by the fact that in the neck region, the LC molecules are predominantly aligned to the fiber axis. Thus, the viscosity  $\eta_\parallel$  should matter much more than  $\eta_\perp$ . Increasing the viscosity ratio  $\nu$  then amounts to reducing  $\eta_\parallel$  and consequently

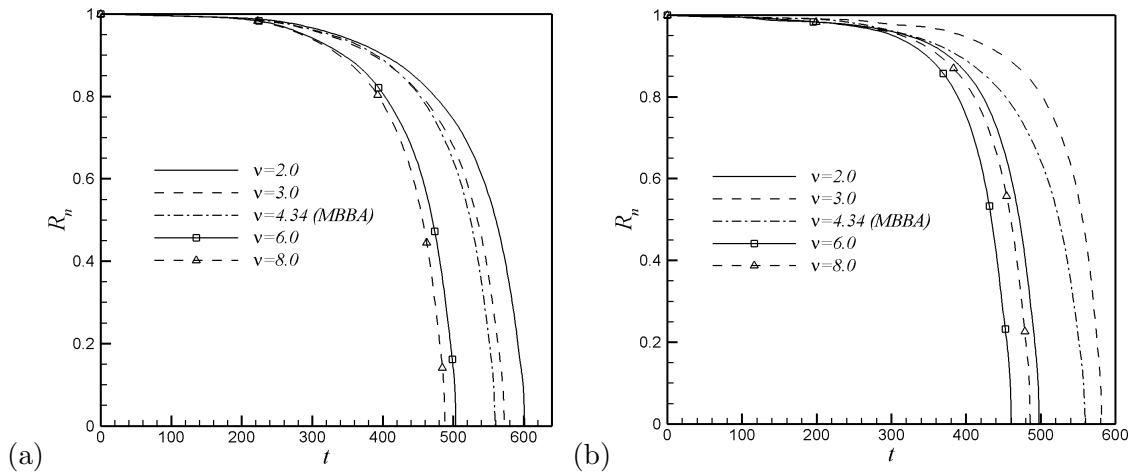


Figure 6: Effect of viscous anisotropy on the thinning of the neck during the breakup of nematic fibers. The average LC viscosity  $\eta$  is fixed such that  $Ca = 1$ ,  $Re = 150$ . In addition,  $A_W = 1$ ,  $A_K = 0.833$ . (a) Varying  $\alpha_2$ ; (b) varying  $\alpha_3$ .

the “effective viscosity” of the ordered LC. The same argument fails for Fig. 6(b), however, where the pinchoff time does not depend on  $\nu$  or  $\alpha_3$  monotonically.

The solution to this puzzle is that the flow within the fiber has both elongation and shear components. While the former dominates at the thinning neck, the higher capillary pressure there drives the fluid toward the wave crest, creating a shear flow that may be likened to the Poiseuille flow. This is illustrated by the axial velocity profiles in Fig. 7. The radial variation  $\partial v_z / \partial r$  gives the degree of shear while the axial one  $\partial v_z / \partial z$  indicates the stretching or compression. Therefore, it is necessary to consider the *elongational viscosity* of the nematic as well. Assuming a uniform director field perfectly aligned with the stretching direction,  $\mathbf{n} = (0, 0, 1)$  in cylindrical coordinates, the stress tensor in the nematic undergoing uniaxial elongation along  $z$  can be calculated from Eq. (6):

$$\sigma' = \text{diag} \left[ -\frac{\alpha_4 \dot{\epsilon}}{2}, -\frac{\alpha_4 \dot{\epsilon}}{2}, (\alpha_1 + \alpha_4 + \alpha_5 + \alpha_6) \dot{\epsilon} \right], \quad (21)$$

where  $\dot{\epsilon}$  is the strain rate. Note that  $\alpha_2$  and  $\alpha_3$  represent rotational friction and do not appear here. Thus, an elongational viscosity can be defined from the normal stress difference

$$\eta_{\parallel}^e = \alpha_1 + \frac{3}{2} \alpha_4 + \alpha_5 + \alpha_6 = \left( 4\eta + \alpha_1 - \frac{\alpha_4}{2} \right) + \alpha_2 - \alpha_3, \quad (22)$$

where we have invoked the average shear viscosity  $\eta$  and the Onsager relation. When we increase  $\nu$  by decreasing  $\alpha_2$  in Fig. 6(a), the elongational viscosity  $\eta_{\parallel}^e$  decreases together

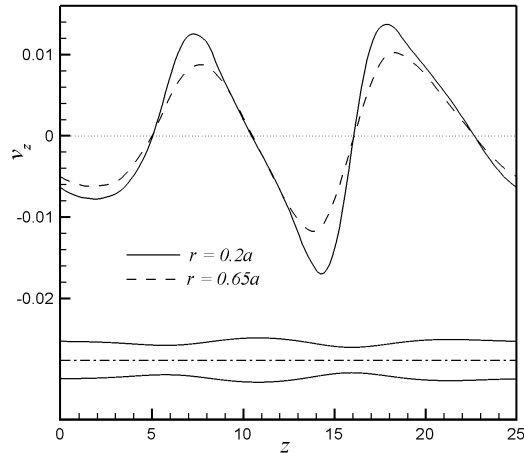


Figure 7: Axial velocity profiles  $v_z(z)$  at two radial positions  $r = 0.2a$  and  $0.65a$  at dimensionless time  $t = 499$ .  $A_W = 1$ ,  $A_K = 0.833$ , and the viscosities correspond to  $\nu = 4.34$  in Fig. 6(a). The velocity is made dimensionless by  $\sigma/\eta$ , and the outline of the fiber at this instant is also shown.

with the “effective shear viscosity” mentioned above. The consequence is unequivocal: the fiber breaks up more rapidly. In Fig. 6(b), on the other hand, increasing  $\nu$  by decreasing  $\alpha_3$  tends to reduce the effective shear viscosity, but in the meantime raises the elongational viscosity. The non-monotonic effect on the breakup of the nematic fiber, therefore, can be interpreted as the outcome of the competition between these two mechanisms.

#### IV. CONCLUSION

In this paper we have investigated the breakup of nematic fibers with planar anchoring on the surface and initially axial molecular orientation in the bulk. The process is simulated from the onset of linear disturbances to nonlinear growth and finally to formation of drops. The main findings can be summarized as follows:

(a) Interface anchoring and bulk elasticity conspire to dampen the growth of capillary waves and the breakup process. In particular, the threshold wavelength for instability is raised and the growth rate of unstable modes is suppressed.

(b) Anisotropic viscosity plays a significant role in the growth of the capillary wave. The effect of individual Leslie coefficients depends on how it changes the elongational and shear viscosities of the nematic liquid crystal separately since both types of flow are involved in the breakup.

(c) The nonlinear growth of the capillary waves leads to the loss of axial periodicity and eventually the formation of polydisperse daughter drops. The nematic order within the fiber does not change the main features of the breakup, besides the quantitative effect of slowing down the process. On the other hand, the interfacial deformation and fluid flow do have a direct effect on the molecular orientation: the nematic is highly aligned in the neck region, and typically displays the bipolar configuration in the daughter drops.

(d) The numerical results are in reasonable agreement with prior work in the literature where comparisons can be made. Specifically, the effect of bulk elasticity and anchoring in suppressing capillary instability is in qualitative agreement with linear analysis. The numerically predicted breakup process captures the main features of experimental observations, and agrees with the latter in that nematic fibers break up in basically the same way as Newtonian ones.

In comparison with linear instability analysis, numerical simulations have the advantage of accessing the later stage of the breakup process. A disadvantage, however, is that the finite domain size tends to influence the wavelength that emerges. Comparison with linear analysis shows quantitative differences because of this restriction. Besides, this work leaves out several physical factors, including homeotropic or more general anchoring directions, bulk textures (radial or onion), non-axisymmetric modes of instability and finally the role of molecular order parameter. The first 3 have been analyzed in the linear limit.<sup>21</sup> The last is known to be relevant to the banded textures observed in nematic fiber breakup.<sup>14</sup> These are open issues that future work should explore.

Nevertheless, this study appears to be the first to explore the nonlinear stage of the capillary breakup and drop pinchoff, and to include all the three factors—anchoring, bulk elasticity and viscous anisotropy—in a self-contained nemato-hydrodynamic theoretical framework. The results will be particularly relevant to the processing and manipulation of nano-scale nematic fibers whose small dimension accentuates distortional elasticity relative to interfacial tension.

**Acknowledgment:** This work was partially supported by the NSERC, the Canada Research Chair program, the Canada Foundation for Innovation and the NSFC (No. 50390095). C.Z. acknowledges partial support by a University Graduate Fellowship from UBC.

## References

- <sup>1</sup> M. Mucha, “Polymer as an important component of blends and composites with liquid crystals,” *Prog. Polym. Sci.* **28**, 837 (2003).
- <sup>2</sup> D. Dutta, H. Fruitwala, A. Kohli, and R. A. Weiss, “Polymer blends containing liquid crystals: A review,” *Polym. Eng. Sci.* **30**, 1005 (1990).
- <sup>3</sup> W. A. Kernick and N. J. Wagner, “The role of liquid-crystalline polymer rheology on the evolving morphology of immiscible blends containing liquid-crystalline polymers,” *J. Rheol.* **43**, 521 (1999).
- <sup>4</sup> D. Acierno and A. A. Collyer, *Rheology and Processing of Liquid Crystal Polymers* (Chapman and Hall, New York, 1996).
- <sup>5</sup> G. Srinivasan and D. H. Reneker, “Structure and morphology of small diameter electrospun aramid fibers,” *Polym. Int.* **36**, 195 (1995).
- <sup>6</sup> D. H. Reneker and I. Chun, “Nanometre diameter fibres of polymer, produced by electrospinning,” *Nanotech.* **7**, 216 (1996).
- <sup>7</sup> B. D. Hamlington, B. Steinhaus, J. J. Feng, D. Link, M. J. Shelley, and A. Q. Shen, “Liquid crystal droplet production in a microfluidic device,” *Liq. Cryst.* **34**, 861 (2007).
- <sup>8</sup> H. A. Stone, A. D. Stroock, and A. Ajdari, “Engineering flows in small devices: Microfluidics toward a lab-on-a-chip,” *Annu. Rev. Fluid Mech.* **36**, 381 (2004).
- <sup>9</sup> P. Yue, J. J. Feng, C. Liu, and J. Shen, “Interfacial force and Marangoni flow on a nematic drop retracting in an isotropic fluid,” *J. Colloid Interface Sci.* **290**, 281 (2005).
- <sup>10</sup> Y. A. Nastishin, H. Liu, T. Schneider, V. Nazarenko, R. Vasyuta, S. V. Shiyanovskii, and O. D. Lavrentovich, “Optical characterization of the nematic lyotropic chromonic liquid crystals: Light absorption, birefringence, and scalar order parameter,” *Phys. Rev. E* **72**, 041711 (2005).
- <sup>11</sup> C. Zhou, P. Yue, J. J. Feng, C. Liu, and J. Shen, “Heart-shaped bubbles rising in anisotropic liquids,” *Phys. Fluids* **19**, 041703 (2007).

- <sup>12</sup> C. Zhou, P. Yue, and J. J. Feng, “The rise of Newtonian drops in a nematic liquid crystal,” *J. Fluid Mech.* **593**, 385 (2007).
- <sup>13</sup> S. Khullar, C. Zhou, and J. J. Feng, “Dynamic evolution of topological defects around drops and bubbles rising in a nematic liquid crystal,” *Phys. Rev. Lett.* **99**, 237802 (2007).
- <sup>14</sup> V. T. Tsakalos, P. Navard, and E. Peuvrel-Disdier, “Observations of the break-up of liquid crystalline polymer threads imbedded in an isotropic fluid,” *Liq. Cryst.* **21**, 663 (1996).
- <sup>15</sup> A. G. C. Machiels, J. V. Dam, A. P. de Boer, and B. Norder, “Stability of blends of thermotropic liquid crystalline polymers with thermoplastic polymers,” *Polym. Eng. Sci.* **37**, 1512 (1997).
- <sup>16</sup> A. D. Rey, “Linear stability theory of break-up dynamics of nematic liquid crystalline fibers,” *J. Phys. II France* **7**, 1001 (1997).
- <sup>17</sup> A. Rapini and M. Popoular, “Distortion d’une lamelle nématique sous champ magnétique conditions d’ancrage aux parois,” *J. Phys. (Paris) C* **30**, 54 (1969).
- <sup>18</sup> Q. Wang, “Role of surface elasticity in capillary instability of cylindrical jets of nematic liquid crystalline polymers,” *J. Non-Newtonian Fluid Mech.* **100**, 97 (2001).
- <sup>19</sup> A.-G. Cheong and A. D. Rey, “Capillary instabilities in thin nematic liquid crystalline fibers,” *Phys. Rev. E* **64**, 041701 (2001).
- <sup>20</sup> A.-G. Cheong and A. D. Rey, “Cahn-hoffman capillarity vector thermodynamics for liquid crystal interfaces,” *Phys. Rev. E* **66**, 021704 (2002).
- <sup>21</sup> A.-G. Cheong and A. D. Rey, “Texture dependence of capillary instabilities in nematic liquid crystalline fibres,” *Liq. Cryst.* **31**, 1271 (2004).
- <sup>22</sup> P. Yue, C. Zhou, J. J. Feng, C. F. Ollivier-Gooch, and H. H. Hu, “Phase-field simulations of interfacial dynamics in viscoelastic fluids using finite elements with adaptive meshing,” *J. Comput. Phys.* **219**, 47 (2006).
- <sup>23</sup> P. G. de Gennes and J. Prost, *The Physics of Liquid Crystals* (Oxford, New York, 1993).

- <sup>24</sup> P. Yue, J. J. Feng, C. Liu, and J. Shen, “A diffuse-interface method for simulating two-phase flows of complex fluids,” *J. Fluid Mech.* **515**, 293 (2004).
- <sup>25</sup> P. Yue, J. J. Feng, C. Liu, and J. Shen, “Diffuse-interface simulations of drop coalescence and retraction in viscoelastic fluids,” *J. Non-Newtonian Fluid Mech.* **129**, 163 (2005).
- <sup>26</sup> P. Yue, C. Zhou, and J. J. Feng, “A computational study of the coalescence between a drop and an interface in Newtonian and viscoelastic fluids,” *Phys. Fluids* **18**, 102102 (2006).
- <sup>27</sup> C. Zhou, P. Yue, and J. J. Feng, “Formation of simple and compound drops in microfluidic devices,” *Phys. Fluids* **18**, 092105 (2006).
- <sup>28</sup> C. Zhou, P. Yue, and J. J. Feng, “Dynamic simulation of droplet interaction and self-assembly in a nematic liquid crystal,” *Langmuir* **24**, 3099 (2007).
- <sup>29</sup> F. M. Leslie, “Some constitutive equations for anisotropic fluids,” *Quart. J. Mech. Appl. Math.* **19**, 357 (1966).
- <sup>30</sup> C. Liu and N. J. Walkington, “Approximation of liquid crystal flows,” *SIAM J. Numer. Anal.* **37**, 725 (2000).
- <sup>31</sup> J. L. Ericksen, “Liquid crystals with variable degree of orientation,” *Arch. Rat. Mech. Anal.* **113**, 97 (1991).
- <sup>32</sup> T. Mikami and S. G. Mason, “The capillary break-up of a binary liquid column inside a tube,” *Can. J. Chem. Eng.* **53**, 372 (1975).
- <sup>33</sup> T. A. Kowalewski, “On the separation of droplets from a liquid jet,” *Fluid Dyn. Res.* **17**, 121 (1996).
- <sup>34</sup> E. A. Theisen, M. J. Vogel, C. A. Lopez, A. H. Hirs, and P. H. Steen, “Capillary dynamics of coupled spherical-cap droplets,” *J. Fluid Mech.* **580**, 495 (2007).
- <sup>35</sup> P. Yue, C. Zhou, and J. J. Feng, “Spontaneous shrinkage of drops and mass conservation in phase-field simulations,” *J. Comput. Phys.* **223**, 1 (2007).
- <sup>36</sup> P. K. Notz, A. U. Chen, and O. A. Basaran, “Satellite drops: Unexpected dynamics and change of scaling during pinch-off,” *Phys. Fluids* **13**, 549 (2001).

- <sup>37</sup> Y. Christanti and L. M. Walker, “Surface tension driven jet break up of strain-hardening polymer solutions,” *J. Non-Newtonian Fluid Mech.* **100**, 9 (2001).
- <sup>38</sup> R. Yu, W. Yu, C. Zhou, and J. J. Feng, “Dynamic interfacial properties between a flexible isotropic polymer and a TLCP investigated by an ellipsoidal drop retraction method,” *J. Appl. Polym. Sci.* **94**, 1404 (2004).
- <sup>39</sup> J.-W. Kim, H. Kim, M. Lee, and J. J. Magda, “Interfacial tension of a nematic liquid crystal/water interface with homeotropic surface alignment,” *Langmuir* **20**, 8110 (2004).
- <sup>40</sup> J. Wu and P. T. Mather, “Interfacial tension of a liquid crystalline polymer in an isotropic polymer matrix,” *Macromol.* **38**, 7343 (2005).
- <sup>41</sup> A. V. Kaznacheev, M. M. Bogdanov, and A. S. Sonin, “The influence of anchoring energy on the prolate shape of tactoids in lyotropic inorganic liquid crystals,” *J. Exp. Theor. Phys.* **97**, 1159 (2003).